Front. Earth Sci. 2019, 13(4): 848–858
https://doi.org/10.1007/s11707-019-0787-3

RESEARCH ARTICLE

Numerical investigation of the wind environment around tall buildings in a central business district

Pingzhi FANG (✉)[1], Deqian ZHENG[2], Ming GU[3], Haifeng CHENG[4], Bihong ZHU[4]

1 Shanghai Typhoon Institute of China Meteorological Administration, Shanghai 200030, China
2 School of Civil Engineering and Architecture, Henan University of Technology, Zhengzhou 450001, China
3 State Key Laboratory for Disaster Reduction in Civil Engineering, Tongji University, Shanghai 200092, China
4 Shanghai Investigation, Design &Research Institute Co., Ltd., Shanghai 200335, China

Abstract The wind environment around tall buildings in a central business district (CBD) was numerically investigated. The district covers an area of ~4.0 km^2 and features a high density of tall buildings. In this study, only buildings taller than 20 m were considered, resulting in 173 tall buildings in the analysis. The numerical investigation was realized using the commercial computational fluid dynamics code FLUENT with the realizable $k-\varepsilon$ turbulence model. Special efforts were made to maintain inflow boundary conditions throughout the computational domain. The reliability of the numerical method was validated using results from an experimental investigation conducted in the core area of the CBD (~1.5 km^2). Experimental and numerical investigations of wind speed ratios at the center of the three tallest buildings in the CBD agree within an uncertainty factor of 2.0. Both the experimental and numerical results show that wind speed ratios in the wind field with exposure category D are higher than those from the wind field with exposure category B. Based on the above validation work, the wind environment around tall buildings in the whole CBD was then investigated by numerical simulation. Common flow phenomena and patterns, such as stagnation points, shielding effects, separation flow, and channeling flow, were identified around the tall buildings. The pedestrian-level wind environment around tall buildings in the CBD was further evaluated using nearby meteorological wind data. The evaluation results show that some pedestrian activities, such as sitting at the center of the three tallest buildings, are unadvisable when the wind blows from the south-east.

Received January 23, 2019; accepted August 16, 2019

E-mail: freedomfpz@163.com

Keywords wind environment, pedestrian-level wind, computational fluid dynamics, wind speed ratio, central business district

1 Introduction

Tall buildings can introduce uncomfortable or even dangerous wind environment at the pedestrian level (Xu et al., 2017). Pedestrian–level wind (PLW) environment, or wind environment around buildings, is a continued topic that needs to be investigated with efforts (Blocken and Stathopoulos, 2013; Blocken, 2014; Blocken et al., 2016; Shen et al., 2017; Zhang et al., 2018). Traditionally, wind environment around buildings was primarily investigated using experimental methods (Blocken and Carmeliet, 2008; Tsang et al., 2012; Zheng et al., 2016). With advances in computational capacity, numerical methods based on computational fluid dynamics (CFD) have become available in recent decades as a complementary tool to investigate wind flow around buildings (Murakami, 1997; Blocken, 2014). Numerical methods have the advantage of low cost and each quantity of interest can be obtained for every location in the computational domain rather than being sampled at only a few locations. The advantages are more notable in the study of the PLW environment. In this respect, PLW environment is one of the few topics in computational wind engineering where nature is kind to us concerning turbulent flows (Ferziger, 1990; Blocken, 2014; Blocken et al., 2016).

Three approaches are used for solving the Navier-Stokes equations numerically: direct numerical simulation (DNS), large eddy simulation (LES), and Reynolds-averaged Navier-Stokes (RANS) simulation. The DNS is a simulation in which the Navier-Stokes equations are numerically solved without any turbulence model. It was often applied

to the generic problems for its expensive costs in the past (Jitendra et al., 2014). The LES is an approach in which the small scales of the flow are removed through a filtering operation, and their effects are modeled using sub-grid scale models. It has been applied in some engineering practices recently (He and Song, 1999; Razak et al., 2013; Tolias et al., 2018) and is seemed as a topic on the assessment of PLW environment in the future (Blocken and Stathopoulos, 2013). The RANS equations are derived by averaging the Navier-Stokes equations. Only the mean flow is solved while all scales of the turbulence are modeled using various kinds of turbulence models in the RANS simulation. Although the RANS approach in computational wind engineering has several important limitations, it has the advantage of low-cost and appears to be rather successful for the study on the PLW environment (Stathopoulos and Baskaran, 1996; Zhang et al., 2005; Vernay et al., 2015; Blocken et al., 2016).

The wind environment around tall buildings in a central business district (~4.0 km^2) was investigated using the commercial CFD code FLUENT with the realizable $k-\varepsilon$ turbulence model. Special efforts were made to maintain inflow boundary conditions (BCs) throughout the computational domain. The reliability of the numerical method was validated by an experimental investigation conducted in a small area of the CBD (~1.5 km^2). This paper is organized as follows. A brief description of the study area and the tall buildings is presented in Section 2. Then, the experimental study of a small area of the CBD (~1.5 km^2) and the numerical simulation methods are presented in Sections 3 and 4, respectively. In Section 5, a numerical simulation of the small experimental area is described. The reliability of the RANS-based method is discussed by comparison with the experimental results for wind speed ratios at the center of the three tallest buildings. Common flow phenomena and patterns at the pedestrian level around tall buildings in the whole CBD, as identified using numerical simulations, are presented in Section 6. The PLW environment is evaluated in reference to nearby meteorological wind data in Section 7. Finally, the conclusions are presented in Section 8.

2 Study area and selected tall buildings

The study area, which is adjacent to the Huangpu River, is a CBD enclosed by the blue circle shown in Fig. 1(a). An enlarged view of the CBD is shown in Fig. 1(b), in which two enclosed areas are identified. The first area (AREA 1), enclosed by two thin black lines and the shoreline of the Huangpu River, is about 1.5 km^2. Totally, there are 57 main buildings higher than 20 m in AREA 1; however, only 40 main buildings were considered for the simplicity in the experimental study. The experimental study on the wind environment around buildings in AREA 1 is mainly used to validate the present numerical method. The second area (AREA 2) is about 4.0 km^2 and is enclosed by two thick blue lines and the shoreline of the Huangpu River. A larger area would provide more realistic aerodynamic information on the evaluation of wind environment. There are totally 173 main buildings higher than 20 m in AREA 2, as shown in Fig. 1(c). The sign "+" in Fig. 1(c) is the origin used in the numerical simulation; and the sign "×" denotes the central position of the three tallest buildings, where the PLW environment is evaluated in the study. As shown in Fig. 1(c), the three tallest buildings in the CBD are the Shanghai Jinmao Tower (SJM), the Shanghai World Financial Center (SWFC) and the Shanghai Tower (SHT, the second tallest building in the world currently, constructed in the year of 2015).

3 Experimental study

An experimental investigation of the wind environment around tall buildings in AREA 1 was conducted in an atmospheric boundary layer (ABL) wind tunnel in Southwest Jiaotong University (Fig. 2). The cross section of the wind tunnel is 22.5 m × 4.5 m with a test length of 36 m. Two different wind fields with exposure categories of B and D were physically simulated according to GB50009-2012 (2012), and the corresponding power law indexes are 0.15 and 0.30, respectively. Wind fields with a scale ratio of 1:300 were realized by using the spires and roughness elements. The reference wind speed is $U_R = 8$ m/s at a height $z_R = 1.8$ m. All the building models were made by the foam according to the aerodynamic shape of the studied buildings. The three tallest building models were further reinforced by steel sticks in the model center. The hot wire anemometers manufactured by DANTEC were placed at the center of the three tallest building models. Wind speeds in the horizontal plane were measured at the height of 0.2 m, 0.3 m, 0.5 m, and 0.7 m, respectively (in model scale). Eight cases were studied for each exposure category, corresponding to eight wind directions: north (N), north-east (NE), east (E), south-east (SE), south (S), south-west (SW), west (W), and north-west (NW).

4 Numerical simulation method

A numerical investigation at a scale ratio of 1:300 was conducted using the commercial CFD code FLUENT (ANSYS 19) with the realizable k-ε turbulence model. All computations were conducted in the Cartesian coordinate system$O$-xyz, where x is the stream-wise direction, y is the lateral direction, z is the vertical direction, and O is the origin, as shown in Fig. 1(c). The optimized computational domain is $-5H \leqslant x \leqslant 10H, -6H \leqslant y \leqslant 6H$ and $0 \leqslant z \leqslant 4H$. The reference height is $H = 1.33$ m, which corresponds to the height of the SJM model. Tetrahedral and hexahedral elements were created. In total, 10 and 16 million elements

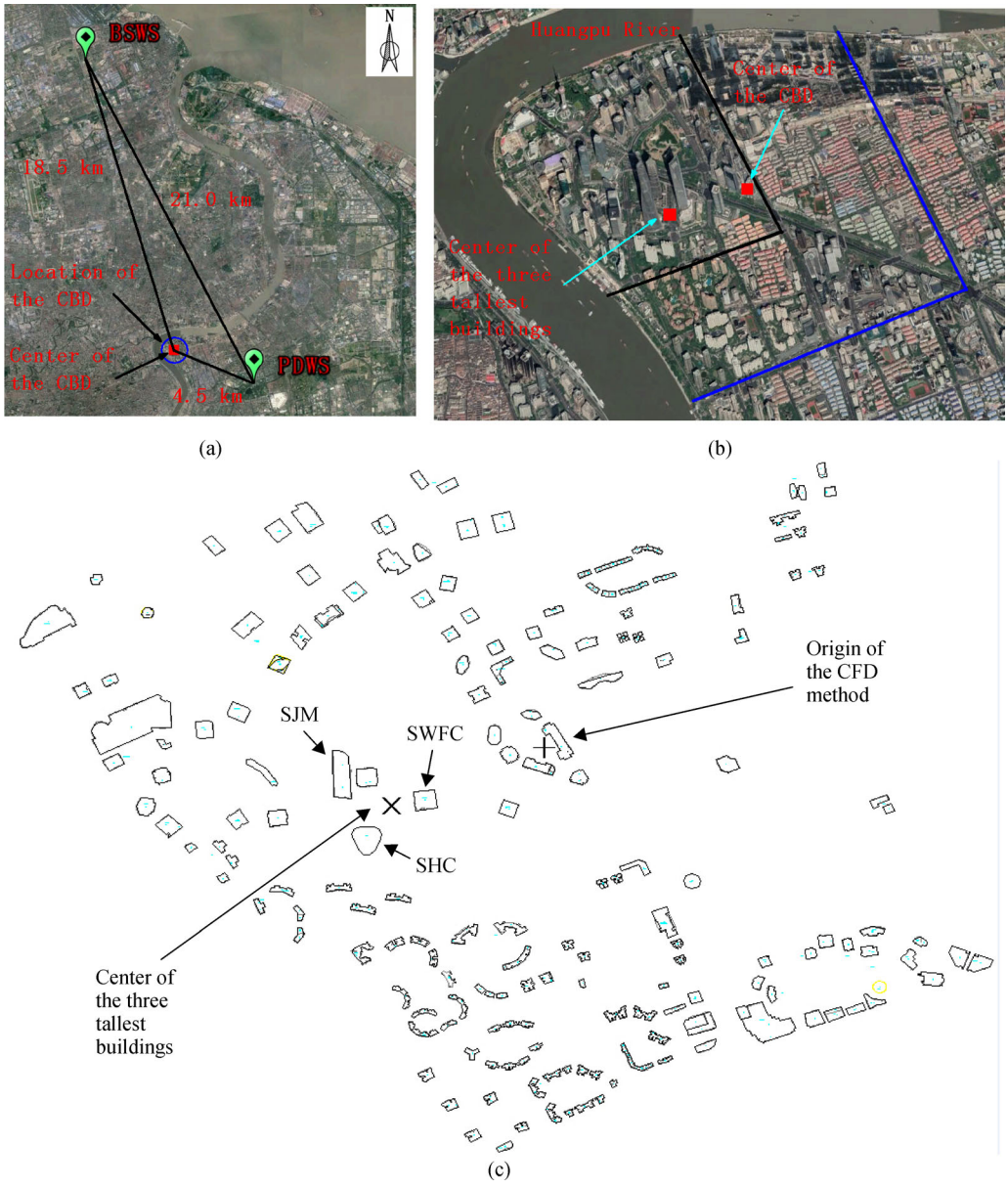

Fig. 1 (a) Location of the CBD and meteorological weather stations; (b) enlarged view of the CBD based on the Baidu map; and (c) buildings taller than 20 m in the CBD (AREA 2).

were generated for AREA 1 and AREA 2 in the overall computational domain, respectively. A Green-Gauss node-based solver was used for accuracy. SIMPLEC was selected for the velocity-pressure decoupled method, and PRESTO and third-order MUSCL discretization methods were adopted for the pressure and momentum equations, respectively. The computation was stopped when the residual error of all physical quantities less than 1.0×10^{-3}. Default options were used for the remaining model settings. In the numerical simulations, the BCs for the computational domain boundaries were set as follows: the velocity-inlet BCs were set at the inlet boundary, the pressure-outlet BCs at the outlet boundary, the wall BCs at the land and the building surfaces, and the symmetry BCs at the top and side boundaries. Special efforts were made to maintain the velocity-inlet BCs throughout the computational domain to reproduce a neutral ABL for the numerical simulations, which are briefly described as follows.

In RANS-based simulations, the standard wall function proposed by Launder and Spalding (1974) is widely adopted. A wall function problem, which underlies the difference between the inlet and approaching flows, may exist when simulating a neutral ABL with a large

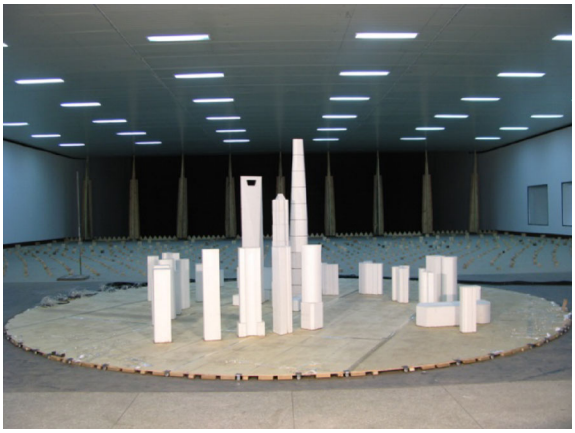

Fig. 2 Experimental investigation of the wind environment around tall buildings in AREA 1.

aerodynamic roughness length using the standard wall function (Blocken et al., 2007b). Much research has been performed on the wall function problem in modeling the neutral ABL (Juretic and Kozmar, 2014; Cindori et al., 2018). Originally, the standard wall function considered uniform roughness elements distributed regularly on a surface. In reality, roughness elements on land surfaces are non-uniform and distributed irregularly. An extra term is thus necessary to resolve the wall function problem when simulating a neutral ABL, as follows (Fang et al., 2015):

$$\frac{U}{u_*} = \frac{1}{\kappa}\ln\frac{z}{K_s} + C_2 - \delta B, \tag{1}$$

where U is the velocity in the stream–wise direction, u_* is the friction velocity, z is the height above the land surface, $\kappa = 0.42$ and $C_2 = \text{const}$, K_s is the physical roughness height, and $\delta B = (\ln\beta)/\kappa$. The parameter β in $z_0' = z_0/\beta$ is often larger than 1.0, which means that the standard wall function with the extra term produces smaller mean wind speeds, as is necessary for simulating a neutral ABL with a large aerodynamic roughness length z_0. Equation (1) reduces to the standard wall function when $\beta = 1$. The extra term can be set by the user-defined function (UDF) in FLUENT. The turbulence model constants and BCs needed to maintain the prescribed velocity-inlet BCs throughout the computational domain are listed in Tables 1–3. As an example, simulation results for profiles of mean wind speed and turbulent kinetic energy for wind fields with exposure categories B and D are shown in Fig. 3. The profiles are from the case when the wind blows from the north (case N for AREA 1). Good agreement was found between the approaching flow ($X = -3.75H$) before the CBD and the prescribed inlet flow ($X = -5.0H$) at the inlet boundary, indicating that the method is able to maintain the velocity-inlet BCs throughout the computational domain.

5 Reliability of the numerical method

The reliability of the numerical method is evaluated by comparison with the experimental results for wind speed ratios at the center of the three tallest buildings. The numerical simulation was conducted for the core area (AREA 1), which corresponds to the experimental area. The wind speed ratio is frequently used in the study of PLW environment and is defined as

Table 1 Model constants for the realizable $k-\varepsilon$ turbulence model at 1:300 scale

Wind field			Model constant		
Exposure category	z_0 /m	z_0' /m	C_2	σ_ε	σ_k
B ($\alpha = 0.15$)	0.0002638	—	1.9	1.2	0.4
D ($\alpha = 0.30$)	0.006756	0.0003556	1.7	1.8	1.0

Table 2 BCs for the wind field with exposure category B at 1:300 scale

Boundary	BC	Mathematical implication	
Inlet	Velocity-Inlet	U	$U = 0.249\ln(z/z_0)/0.42$
		k [a)]	$k = \sqrt{-0.0040\ln(z/z_0) + 0.0354}$
		ε	$\varepsilon = C_\mu^{1/2} k\partial U/\partial z$, $C_\mu = 0.13$
Outlet	Pressure-Outlet	k, ε: same as those at the inlet boundary	
Top	Symmetry	$\partial(U, P, k, \varepsilon)/\partial z = 0$	
Side	Symmetry	$\partial(U, P, k, \varepsilon)/\partial y = 0$	
Building surface	Wall	Standard wall function (SWF): $K_s = 0$	
Land surface	Wall	Standard wall function (SWF): $K_s = 6.5z_0$	

[a)] The equation for κ is from Yang et al. (2009).

Table 3 BCs for the wind field with exposure category D at 1:300 scale

Boundary	BC	Mathematical implication	
Inlet	Velocity-Inlet	U	$U = 0.4018\ln((z+z_0)/z_0)/0.42$
		k [a)]	$k = \sqrt{-0.013\ln((z+z_0)/z_0)+0.075}$
		ε	$\varepsilon = C_\mu^{1/2} k\partial U/\partial z$, $C_\mu = 0.09$
Outlet	Pressure-Outlet	k, ε: same as those at the inlet boundary	
Top	Symmetry	$\partial(U, P, k, \varepsilon)/\partial z = 0$	
Side	Symmetry	$\partial(U, P, k, \varepsilon)/\partial y = 0$	
Building surface	Wall	Standard wall function (SWF): $K_s = 0$	
Land surface	Wall	User-defined WF with $\delta B = 7.0$ and $K_s = 6.5z_0'$	

[a)] The equation for k is from Yang et al. (2009).

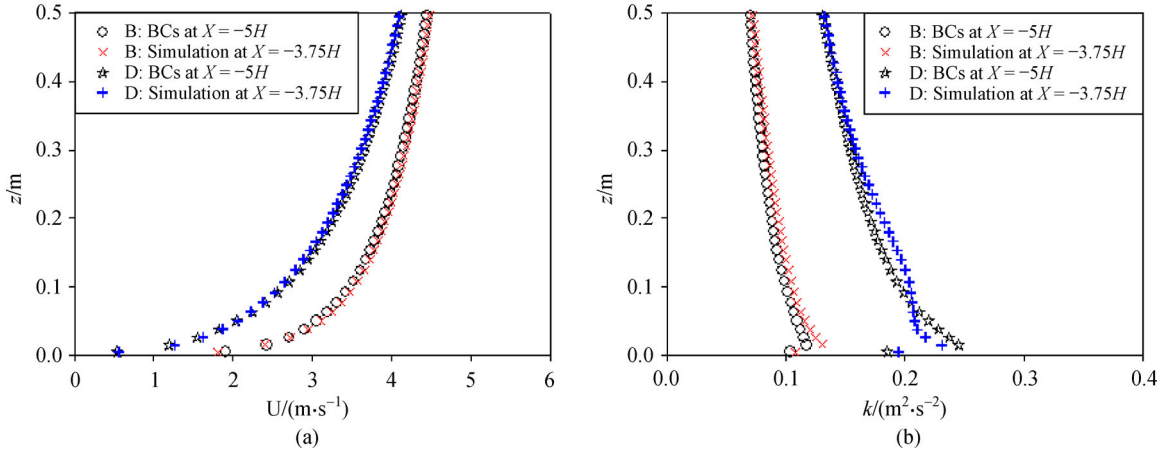

Fig. 3 Comparisons of profiles of the prescribed inlet flow at the inlet boundary ($X = -5.0H$) and the approaching flow before the CBD ($X = -3.75H$), for wind fields with exposure categories B and D: (a) profiles of the mean wind speed; and (b) profiles of the turbulent kinetic energy.

$$R_i = \frac{U_i}{U_{\text{ref}}}, \tag{2}$$

where U_i is the wind speed at measurement point i and U_{ref} is the undisturbed wind speed at the same height.

Wind speed ratios at the center of the three tallest model buildings, from the wind tunnel and numerical results for wind fields with each exposure category, are compared in Fig. 4. Four points were measured vertically for each case in the wind tunnel tests; thus, there are 28 measurement points for seven cases (case E was removed because of corrupted data) for wind fields with each exposure category. The wind speed ratios are mostly smaller than 1.0, which means that the area at the center of the three tallest buildings is shielded by the buildings. The numerical results are 1.2336 times higher than the wind tunnel results for the wind field with exposure category B, and 1.3570 times higher for the wind field with exposure category D. The mean numerical results are 1.30 times higher than the wind tunnel results within an uncertainty factor of 2.0 (with deviation ranges normalized by the ideal value), as shown by the blue dashed and dotted lines in Fig. 4. Blocken (2014) showed that the uncertainty factor can reach 5.0 or more in the wake region behind buildings, where the wind speed ratios are smaller than 1.0. In addition to deficiencies in turbulence models used in numerical methods (Blocken, 2014), these differences can also be attributed to the mismatched simulation on the wind fields and the relative positions of the measurement points to the building models between the wind tunnel and numerical methods. For example, an inhomogeneity of the wind field in the lateral direction was observed in the wind tunnel tests ($\partial U/\partial y \neq 0$); however, an ideal wind field exists in the numerical simulations ($\partial U/\partial y = 0$). In addition, wind speed ratios in the wind field with exposure category D are 1.10 times higher than those in the wind field with exposure category B in the wind tunnel, and are 1.27 times higher in the numerical simulations (Fig. 5). This phenomenon is more noticeable for wind speed ratios near the ground, as shown in Fig. 6. These results clearly demonstrate the effects of exposure category and roughness on wind speed ratios. Therefore, an appropriate

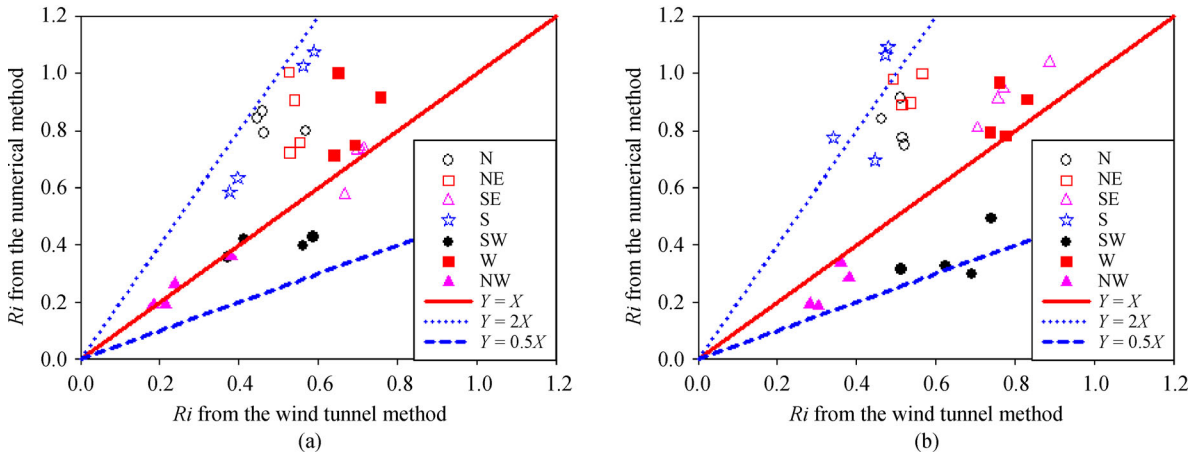

Fig. 4 Comparisons of the wind speed ratios between the wind tunnel and numerical results: (a) results from the wind field with exposure category B; and (b) results from the wind field with exposure category D.

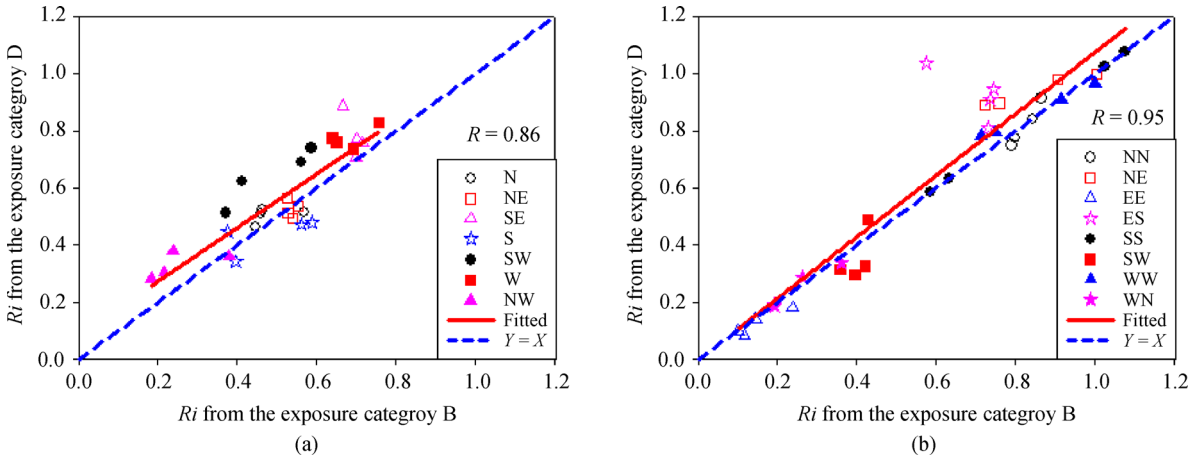

Fig. 5 Comparisons of the wind speed ratios between the wind fields with different exposure categories: (a) wind tunnel results; and (b) numerical results.

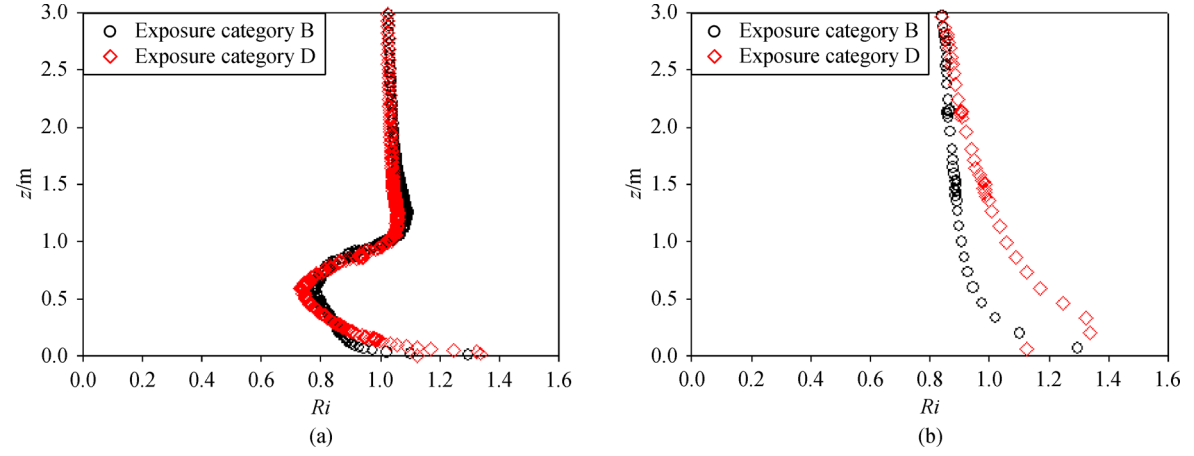

Fig. 6 Numerical results on the variation of the wind speed ratios with height for the case N: (a) the whole profile; and (b) profile near the land surface.

exposure category should first be determined in the study of wind environment. According to GB50009-2012 (2012), a wind field with exposure category D was chosen for this study on wind environment in the CBD (AREA 2).

6 Common flow phenomena and patterns around tall buildings

The wind environment around tall buildings in the CBD (AREA 2) was investigated using numerical results from the wind field with exposure category D. Aerodynamic shapes of the buildings and the mesh scheme on the land and building surfaces were shown in Fig. 7. For simplicity, only representative computational results for wind speed ratios at a height $h = 0.0067$ m (corresponding to a height of 2.0 m at full scale) from cases N and SE are shown in Fig. 8. Local areas of lower wind speed ratio (< 1.0) are prevalent on the downwind sides of the buildings, particularly in downwind areas of the CBD. This is due to a shielding effect caused by the tall buildings. Other areas with lower wind speed ratios appear on the upwind sides of buildings. This is caused mainly by a stagnation effect, where the flow is nearly frozen at the stagnation point. In areas with lower wind speed ratios, air quality is worse because of weak convection of the pollutant particles and the exhausted gases. Local areas of higher wind speed ratio (> 1.0) are prevalent in passageways between buildings, particularly in upwind areas of the CBD. This is caused mainly by channeling flow, other than the Venturi effect, as pointed out by Blocken et al. (2007a). Other areas of higher wind speed ratio are located at the upwind corners of buildings, where separation flow dominates. Areas with higher wind speed ratios are potentially hazardous to pedestrians. Another result from the simulation is the observation that higher tall-building density leads to more areas with lower wind speed ratios, as is evident in the lower-left part of the CBD in Fig. 8(b). This is more obvious in Fig. 8(a) for the north-wind case (case N), in which the position of the high density area is shifted toward the downwind area of the CBD.

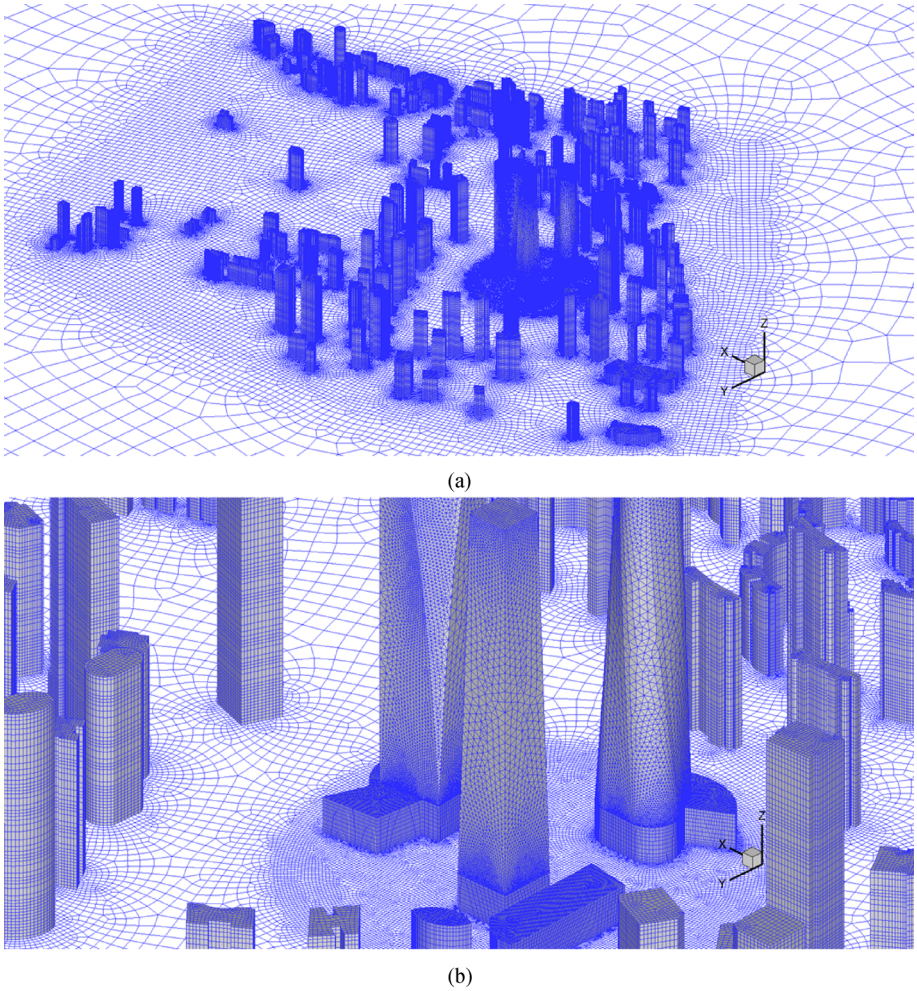

(a)

(b)

Fig. 7 (a) Aerodynamic shapes of the buildings and the mesh scheme on the land and building surfaces; (b) close view around the three tallest buildings.

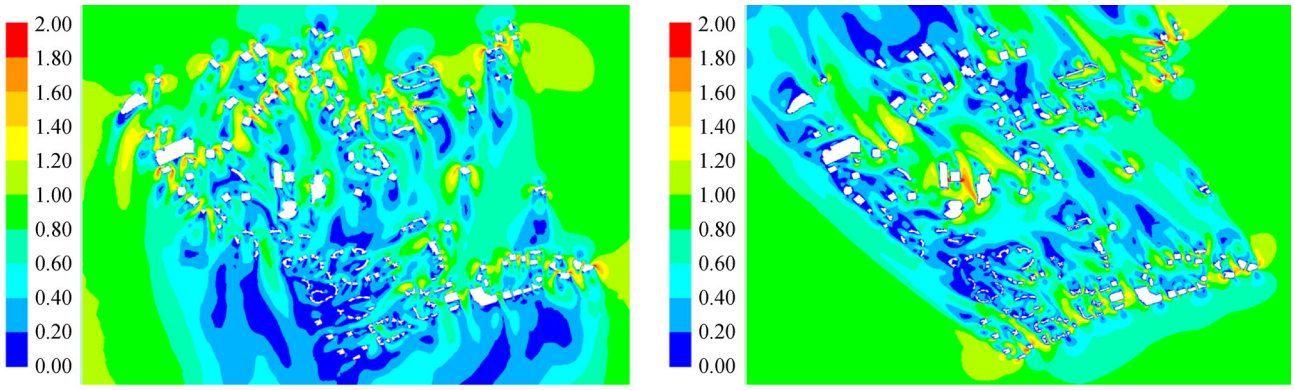

Fig. 8 Contours of wind speed ratios at the pedestrian level $h = 0.0067$m (corresponding to a height of 2.0 m at full scale) for (a) case N; and (b) case SE.

7 Evaluation of the PLW environment

Numerical simulations were applied to an evaluation of the PLW environment at the center of the three tallest buildings (SJM, SWFC, and SHT), as shown in Fig. 1(c). The evaluation of the PLW environment involved combining statistical meteorological wind data with aerodynamic information, and wind comfort and wind safety criteria. Aerodynamic information is needed to transform statistical meteorological wind data from a reference weather station to the location of interest at the building site. At this location, the transformed statistical data are combined with the comfort and safety criteria to assess the local wind comfort and safety. The aerodynamic information includes the wind speed ratio calculated according to Eq. (2), as well as the terrain-related transform factor for the change of terrain between the reference weather station and the upwind site of the study area.

7.1 Meteorological wind data and terrain transform factor

Meteorological wind data from two weather stations, the Baoshan Weather Station (BSWS) and the Pudong Weather Station (PDWS), were used to study the PLW environment. As shown in Fig. 1(a), the BSWS and the PDWS are located ~18.5 km north-west and ~4.5 km south-east of the study area, respectively. The distance between the BSWS and PDWS is ~21.0 km. The BSWS is a basic weather station operated by the China Meteorological Administration. The shortest distance from the shoreline to the BSWS is ~5.0 km. Thus, the BSWS is used as a reference weather station in this study. The PDWS is near the study area and was chosen to analyze terrain-related aerodynamic information (i.e., the terrain-related transform factor).

Hourly wind data for 2002–2016 were collected from the BSWS with the averaging time interval of 2 min. Statistical results for the wind data are shown in Fig. 9. The mean, median, and mode wind speeds in each wind direction are nearly identical, as shown in Fig. 9(a). This means that the wind distribution is nearly symmetric. Winds from the east, north-east, south-east, and west prevail, indicating that wind in this area is controlled by the monsoon, as shown in Fig. 9(b). Wind data from the PDWS for 2003–2013 were collected to obtain the terrain-related transform factor T (Table 4). As can be seen in the table, the wind speed near the land surface (typically at height of 10 m) in the downtown area is about 0.586 times of that in the suburban area in a mean sense.

7.2 Comfort and safety criteria, and evaluation results

Comfort and safety criteria developed by Soligo et al. (1998) were adopted in the present study, and are listed in Table 5. Three activities (sitting, standing, and walking) were included in the criteria. For each activity, the wind speed range and a threshold value of occurrence frequency were provided. For example, the occurrence frequency for wind speeds in the range 0–2.5 m/s should be $> 80\%$ for the activity of sitting for each wind direction. The criteria also include occurrence frequency for uncomfortable and severe situations for the PLW evaluation.

According to GB50009-2012 (2012), the topography around the BSWS can be assigned to exposure category B with power law index $\alpha = 0.15$. The height-related conversion factor between 2.0 m and 10.0 m at the reference weather station is $U_{2,\mathrm{WS}}/U_{10,\mathrm{WS}} = 0.786$. Considering the time-related converting factor caused by the

Table 4 Terrain-related transform factor T in each wind direction

Wind direction	N	NE	E	SE	S	SW	W	NW
Transform factor	0.53	0.57	0.61	0.65	0.62	0.55	0.61	0.56

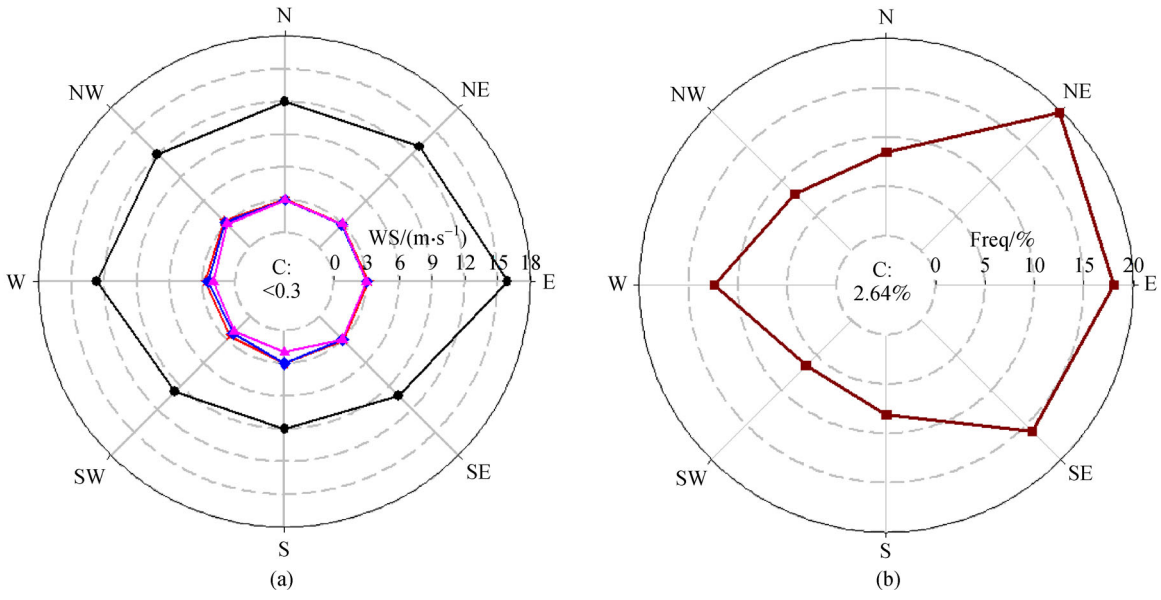

Fig. 9 Wind rose diagrams showing (a) speed; and (b) direction for the BSWS. Calm conditions is denoted 'C' and corresponds to wind speeds of < 0.3 m/s; —●—: maximum wind speed; —★—: mean wind speed; —◆—:median wind speed; —▲—: mode wind speed; and —■—: wind direction.

averaging time interval between 10 min and 2 min, $G_{600,3600}/G_{120,3600} = 0.91$ (Harper et al., 2009), the wind speed $U_{2,\mathrm{IS}}$ at the height of 2 m in-site or at the center of the three tallest buildings can be expressed as follows (Willemsen and Wisse, 2002):

$$U_{2,\mathrm{IS}} = 0.786 \times (R_{i,\mathrm{NUM}} \pm \delta R_{i,\mathrm{NUM}}) \times (T \pm \delta T) \times 0.91 \times U_{10,\mathrm{WS}}, \quad (3)$$

where $R_{i,\mathrm{NUM}}$ is the wind speed ratio caused by the disturbance from adjacent buildings and is derived from the numerical simulation results, and $\delta(\bullet)$ is the measurement error or uncertainty. We set $\delta = 0$ in this study. According to the criteria in Table 5 and Eq. (3), the evaluation of the PLW environment at the center of the three tallest buildings was carried out and the results for each wind direction are presented in Table 6. The activity of sitting is not advisable when the south-east wind blows.

It should be stressed that these results are based on only tall buildings in the CBD. However, the central position is dominated by a separation flow caused by the south-west parts of buildings attached to the SWFC when a south-east wind blows, as shown in Fig. 8(b). Residential buildings with lower heights (< 20 m) are prevalent in the south-east direction, as can be inferred from Fig. 1(c). The real roughness length may be smaller than that in the CFD simulations, leading to higher wind speeds in the downwind direction. Results from this study are thus important, considering the prevalence of south-east winds in the study area.

Table 5 Comfort and safety criteria developed by Soligo et al. (1998)

Activity	Wind speed range/(m·s^{-1})	Occurrence frequency
Sitting	< 2.5	> 80%
Standing	< 3.9	> 80%
Walking	< 5.0	> 80%
Uncomfortable	> 5.0	> 20%
Severe	> 14.4	> 0.10%

Table 6 Evaluation results for the pedestrian-level wind environment [a)]

Wind direction			N	NE	E	SE	S	SW	W	NW
Activity	Sitting	OFreq	99.83°	90.89°	99.96°	67.13°	100°	100°	100°	100°
		EResult	P	P	P	R	P	P	P	P
	Standing	OFreq	100°	99.55°	100°	95.65°	100°	100°	100°	100°
		EResult	P	P	P	P	P	P	P	P
	Walking	OFreq	100°	99.95°	100°	99.54°	100°	100°	100°	100°
		EResult	P	P	P	P	P	P	P	P

[a)] Abbreviations: OFreq, occurrence frequency; EResult, evaluation result; P, passed; and R, rejected.

8 Conclusions

The pedestrian-level wind environment around tall buildings in a CBD was numerically studied using CFD simulations. The area of the CBD is ~4 km^2, and 173 buildings taller than 20 m were considered in the study. The numerical method was validated by comparing simulation results from a small portion of the CBD with those of an experimental study. Common flow phenomena and patterns were identified around buildings in the numerical simulation results. The pedestrian-level wind environment was evaluated at the center of the three tallest buildings. The main conclusions are as follows.

1) Special efforts were made to maintain the inflow boundary conditions throughout the computational domain. Experimental and numerical simulation results for wind speed ratios at the center of the three tallest buildings in the CBD are in agreement within an uncertainty factor of 2.0. The numerical method used here is thus found to accurately simulate wind flow in the CBD, which has a high density of tall buildings.

2) Numerical results clearly demonstrate the effects of exposure category and roughness on wind speed ratios. An appropriate exposure category should thus first be determined in studies of wind environments. A wind field with exposure category D was chosen for this study of the wind environment of the CBD.

3) Local areas of higher wind speed ratio are prevalent in passageways between buildings and near upwind corners of buildings, whereas local areas near the upwind and downwind sides of buildings are dominated by lower wind speed ratios. These are caused mainly by channeling flow, separating flow, stagnation, and shielding effects, respectively. Higher tall-building density increases the areas with lower wind speed ratios, inducing possible air-quality problems due to weak convection of the pollutant particles and the exhausted gases.

4) According to a set of criteria for PLW environment adopted in this study, some pedestrian activities, such as sitting at the center of the three tallest buildings, are unadvisable when the wind is from the south-east. Although these results are based on only tall buildings in the CBD, they should still be treated seriously, considering the separation flow caused by the south-west part of the buildings attached to the SWFC, the higher density of lower residential buildings in the south-east direction of the CBD, and the prevailing south-east wind in the study area.

The ultimate goal of the study was to provide high-resolution numerical wind fields around tall buildings in the CBD and use them as a basis for further studies on, for example, forecasting wind fields coupled with meso-scale WRF model simulations and predictions of the likelihood of glass falling from tall buildings in the CBD under typhoon conditions.

Acknowledgements This research was supported by the Ministry of Science and Technology of the People's Republic of China (Grant Nos. 2015CB452806 and 2018YFB1501104), the National Natural Science Foundation of China (Grant No. 51408196), and the Natural Science Foundation of Shanghai (Grant No. 19ZR1469200). Further support was provided by the State Key Laboratory for Disaster Reduction in Civil Engineering (No. SLDRCE15-A-04) and the Study on the Wind Characteristics Caused by Typhoons Considering Offshore Wind Farm Safety along Fujian Province (No. 2016FD(8)-008). The authors are indebted to the anonymous reviewers who provided valuable suggestions that improved the manuscript, particularly scientific aspects.

References

Blocken B (2014). 50 years of computational wind engineering: past, present, and future. J Wind Eng Ind Aerodyn, 129: 69–102

Blocken B, Carmeliet J (2008). Pedes trian wind conditions at outdoor platforms in a high-rise apartment building: generic sub-configuration validation, wind comfort assessment, and uncertainty issues. Wind Struct, 11(1): 51–70

Blocken B, Carmeliet J, Stathopoulos T (2007a). CFD evaluation of wind speed conditions in passages between parallel buildings-effect of wall-function roughness modifications for the atmospheric boundary layer flow. J Wind Eng Ind Aerodyn, 95(9–11): 941–962

Blocken B, Stathopoulos T (2013). CFD simulation of pedestrian-level wind conditions around buildings: past achievements and prospects. J Wind Eng Ind Aerodyn, 121: 138–145

Blocken B, Stathopoulos T, Carmeliet J (2007b). CFD simulation of the atmospheric boundary layer: wall function problems. Atmos Environ, 41(2): 238–252

Blocken B, Stathopoulos T, van Beeck J P A J (2016). Pedestrian-level wind conditions around buildings: review of wind-tunnel and CFD techniques and their accuracy for wind comfort assessment. Build Environ, 100: 50–81

Cindori M, Juretic F, Kozmar H, Dzijan I (2018). Steady RANS model of the homogeneous atmospheric boundary layer. J Wind Eng Ind Aerodyn, 173: 289–301

Fang P, Gu M, Tan J, Han Z (2015). A method to solve the wall function problem in simulating the atmospheric boundary layer. J Vibration Shock, 34(2): 85–90 (in Chinese)

Ferziger J H (1990). Approaches to turbulent flow computation: applications to flow over obstacles. J Wind Eng Ind Aerodyn, 35: 1–19

GB50009–2012 (2012). National Standard of the People's Republic of China: Load Code for the Design of Building Structures (in Chinese)

Harper B A, Kepert J D, Ginger J D (2009). Guidelines for converting between various windaveraging periods in tropical cyclone conditions. In: Sixth Tropical Cyclone RSMCs/TCWCs Technical Coordination Meeting Technical Document. Brisbane

He J, Song C C S (1999). Evaluation of pedestrian winds in urban area by numerical approach. J Wind Eng Ind Aerodyn, 81(1–3): 295–309

Jitendra T, Zhao M, Zhou T M, Cheng L (2014). Three-dimensional simulation of vortex shedding flow in the wake of a yawed circular cylinder near a plane boundary at a Reynolds number of 500. Ocean Eng, 87(1): 25–39

Juretic F, Kozmar H (2014). Computational modeling of the atmospheric boundary layer using various two-equation turbulence models. Wind Struct, 19(6): 687–708

Launder B E, Spalding D B (1974). The numerical computation of turbulent flows. Comput Methods Appl Mech Eng, 3(2): 269–289

Murakami S (1997). Current status and future trends in computational wind engineering. J Wind Eng Ind Aerod, 67: 3–34

Razak A A, Hagishima A, Ikegaya N, Tanimoto J (2013). Analysis of airflow over building arrays for assessment of urban wind environment. Build Environ, 59: 56–65

Shen L, Han Y, Cai C S, Dong G C, Zhang J R, Hu P (2017). LES of wind environments in urban residential areas based on an inflow turbulence generating approach. Wind Struct, 24(1): 1–24

Soligo M J, Irwin P A, Williams C J, Schuyler G D (1998). A comprehensive assessment of pedestrian comfortincluding thermal effects. J Wind Eng Ind Aerod, 77(1): 753–766

Stathopoulos T, Baskaran A (1996). Computer simulation of wind environmental conditions around buildings. Eng Struct, 18(11): 876–885

Tolias I C, Koutsourakis N, Hertwig D, Efthimiou G C, Venetsanos A G, Bartzis J G (2018). Large Eddy Simulation study on the structure of turbulent flow in a complex city. J Wind Eng Ind Aerodyn, 177: 101–116

Tsang C W, Kwok K C S, Hitchcock P A (2012). Wind tunnel study of pedestrian level wind environment around tall buildings: effects of building dimensions, separation and podium. Build Environ, 49: 167–181

Vernay D G, Raphael B, Smith I F C (2015). Improving simulation predictions of wind around buildings using measurements through system identification techniques. Build Environ, 94(2): 620–631

Willemsen E, Wisse J A (2002). Accuracy of assessment of wind speed in the built environment. J Wind Eng Ind Aerod, 90(10): 1183–1190

Xu X D, Yang Q S, Yoshida A, Tamura Y (2017). Characteristics of pedestrian-level wind around super-tall buildings with various configurations. J Wind Eng Ind Aerod, 166: 61–73

Yang Y, Gu M, Chen S Q, Jin X (2009). New inflow boundary conditions for modelling the neutral equilibrium atmospheric boundary layer in computational wind engineering. J Wind Eng Ind Aerod, 97(2): 88–95

Zhang A, Gao C, Zhang L (2005). Numerical simulation of the wind field around different building arrangements. J Wind Eng Ind Aerod, 93(12): 891–904

Zhang X, Tse K T, Weerasuriya A U, Kwok K C S, Niu J, Lin Z, Mak C M (2018). Pedestrian-level wind conditions in the space underneath lift-up buildings. J Wind Eng Ind Aerod, 179: 58–69

Zheng C R, Li Y S, Wu Y (2016). Pedestrian-level wind environment on outdoor platforms of a thousand-meter-scale megatall building: sub-configuration experiment and wind comfort assessment. Build Environ, 106(9): 313–326